Inorg. Chem. **2007**, *46*, 251–260

Atomic Distributions in the γ-Brass Structure of the Cu–Zn System: A Structural and Theoretical Study

Olivier Gourdon,*,† Delphine Gout,† Darrick J. Williams,† Thomas Proffen,† Sara Hobbs,‡ and Gordon J. Miller‡,§

Los Alamos National Laboratory, Los Alamos, New Mexico 87545, Department of Chemistry, Iowa State University, Ames, Iowa 50011, and Ames Laboratory, Department of Energy, Ames, Iowa 50011

Received August 30, 2006

The crystal structures, atomic distributions, and theoretical electronic structures of five different $Cu_{5-x}Zn_{8+x}$ γ-brass compounds ($x = -0.59(3)$, $-0.31(3)$, 0.00(3), 0.44(3), and 0.79(3)) are reported with the goal of identifying chemical influences on the observed phase width. These structures have been refined by both neutron and X-ray powder diffraction to obtain accurate crystal chemical parameters. All compounds crystallize in the space group $I\bar{4}3m$ (No. 217) ($Z = 4$), and the unit cell parameters are $a = 8.8565(4)$, 8.8612(5), 8.8664(3) , 8.8745(4), and 8.8829(7) Å, respectively, for $Cu_{5.59}Zn_{7.41}$, $Cu_{5.31}Zn_{7.69}$, $Cu_{5.00}Zn_{8.00}$, $Cu_{4.56}Zn_{8.44}$, and $Cu_{4.21}Zn_{8.79}$. The results indicate specific site substitutions on both sides of the ideal composition "Cu_5Zn_8". In all cases, the 26-atom cluster building up the γ-brass structure shows a constant inner $[Cu_4Zn_4]$ tetrahedral star with compositional variation occurring at the outer octahedron and cuboctahedron. First principles and semiempirical electronic structure calculations using both a COHP and Mulliken population analysis were performed to understand the observed compositional range and to address the "coloring problem" for the site preferences of Cu and Zn atoms for this series of compounds.

Introduction

Reinvestigation of the Cu−Zn binary system in the γ-brass region, i.e., between 57 and 68 atom % Zn, is motivated by the relationship between the cubic γ-brass structure and various quasi-crystal approximants.[1−10] γ-Brasses are included among Hume−Rothery electron phases, which achieve their stability by the interaction between the Fermi surface (a sphere with radius k_F in reciprocal space in the free electron model) and the Brillouin zone (the convex polyhedra with faces located at planes perpendicular to $\mathbf{k}/2$, where $\mathbf{k}$ = a reciprocal lattice vector).[11,12] According to Hume−Rothery's principles of electron compounds,[13,14] the cubic

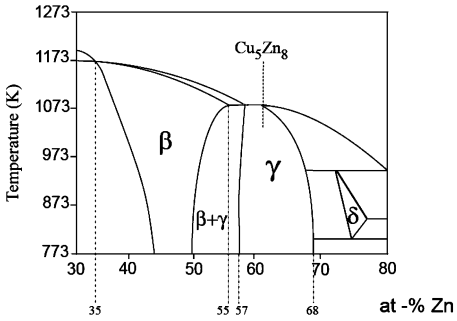

Figure 1. Representation of the Cu−Zn binary phase diagram in the range 30−80 atom % Zn and between 773 and 1273 K. Composition limits for the β and γ brasses are noted, as well as the Cu_5Zn_8 composition.[27,28]

* To whom correspondence should be addressed. E-mail: gourdon@lanl.gov.
† Los Alamos National Laboratory.
‡ Iowa State University.
§ Ames Laboratory.

(1) Demange, V.; Ghanbaja, J.; Machizaud, F.; Dubois, J. M. *Philos. Mag.* **2005**, *85*, 1261.
(2) Demange, V.; Milandri, A.; de Weerd, M. C.; Machizaud, F.; Jeandel, G.; Dubois, J. M. *Phys. Rev. B* **2002**, *B65*, 144205.
(3) Ebalard, S.; Spaepen, F. *J. Mater. Res.* **1991**, *6*, 1641.
(4) Dong, C.; *Philos. Mag. A* **1996**, *A73*, 1519.
(5) Boström, M.; Hovmöller, S. *J. Solid State Chem.* **2000**, *153*, 398.
(6) Ge, S. P.; Kuo, K. H. *J. Mater. Res.* **1999**, *14*, 2799.
(7) Ranganathan, S.; Subramaniam, A.; Tsai, A. P.; Dong, C. *Ferroelectrics* **2001**, *250*, 201.
(8) Demange, V.; Ghanbaja, J.; Beeli, C.; Machizaud, F.; Dubois, J. M. *J. Mater. Res.* **2004**, *19*, 2285.
(9) Gourdon, O.; Izaola, Z.; Elcoro, L.; Petricek, V.; Miller, G. J. *Philos. Mag.* **2006**, *86*, 419.
(10) Gourdon, O.; Miller, G. J. *Chem. Mater.* **2006**, *18*, 1848.
(11) Pearson, W. B. *The Crystal Chemistry and Physics of Metals and Alloys*; Wiley-Interscience: New York, 1972; pp 80−133.
(12) Pettifor, D. G. *Bonding and Structure of Molecules and Solids*; Oxford Science Publications: Oxford, 1995.
(13) Hume-Rothery, W. *J. Inst. Met.* **1926**, *35*, 295, 307.
(14) Hume-Rothery, W.; Mabbott, G. W.; Channel-Evans, K. M. *Philos. Trans. R. Soc., Ser. A* **1934**, *A233*, 1.

10.1021/ic0616380 CCC: $37.00
Published on Web 12/09/2006

Table 1. Compositions, Unit Cell Parameters, Refined Compositions, and Refinement Statistics for $Cu_{5-x}Zn_{8+x}$ ($x = -0.59$, -0.31, 0.00, 0.44, and 0.79)

loaded composition (%)	$Cu_{5.59}Zn_{7.41}$ ($Cu_{43}Zn_{57}$)	$Cu_{5.31}Zn_{7.69}$ ($Cu_{41}Zn_{59}$)	$Cu_{5.00}Zn_{8.00}$ ($Cu_{38.5}Zn_{61.5}$)	$Cu_{4.56}Zn_{8.44}$ ($Cu_{35}Zn_{65}$)	$Cu_{4.21}Zn_{8.79}$ ($Cu_{32.5}Zn_{67.5}$)
EDX composition	$Cu_{5.62(3)}Zn_{7.38(3)}$	$Cu_{5.30(3)}Zn_{7.70(3)}$	$Cu_{4.99(3)}Zn_{8.01(3)}$	$Cu_{4.58(4)}Zn_{8.42(4)}$	$Cu_{4.22(5)}Zn_{8.78(5)}$
X-ray Diffraction					
a (Å)	8.8562(6)	8.8605(3)	8.8674(2)	8.8747(5)	8.8835(6)
R_w	3.78%	3.47%	3.03%	4.02%	3.61%
Neutron Diffraction					
refined composition	$Cu_{5.60(2)}Zn_{7.40(2)}$	$Cu_{5.36(1)}Zn_{7.64(1)}$	Cu_5Zn_8	$Cu_{4.55(2)}Zn_{8.45(2)}$	$Cu_{4.21(2)}Zn_{8.79(2)}$
a (Å)	8.8565(4)	8.8601(5)	8.8664(3)	8.8744(4)	8.8829(7)
χ_2	2.083	1.656	1.682	2.077	2.046

γ-brass phase is preferred for a valence electron concentration (vec = number of valence s and p electrons/number of atoms in the chemical formula) of 1.61 = 21/13 s and p electrons/atom. In the Cu−Zn binary system, this concept leads to the "ideal" composition of "Cu_5Zn_8", i.e., 61.5 atom % Zn. However, a wide range of composition has been observed around both sides of this concentration, although no detailed reports on the distribution of Cu and Zn among the various sites in the crystal structure exist.

Within the nearly free electron theory of electronic structure for metals, the composition range in Cu−Zn γ-brasses is nicely explained by an argument presented by Jones and Mott.[15,16] They constructed a large polyhedral zone, called a "Jones zone", from the 36 {330} and {411} planes in reciprocal space, planes which give large structure factors for the γ-brass structure and could show that the space enclosed accommodates 1.73 "free" valence electrons per atom.[17] This zone is nearly spherical, and an inscribed sphere (i.e., a sphere just touching the polyhedral faces) holds 1.54 free valence electrons per atom.[18] In this picture, the valence d electrons are treated as tightly held by the nuclei and do not contribute to the free electrons; these are assigned to the valence s and p electrons. In the Mott and Jones model, the spherical Fermi surface will be distorted when it approaches the faces of the Jones zone, opening energy gaps in the band structure near these positions in reciprocal space and providing some energetic stabilization relative to other structures (i.e., other translational periodicities).

There remains, however, some controversy regarding the origin of the stability of the γ-brass phases. Paxton et al. assign its stability to a lowering of the density of states around 1.7 electrons per atom.[18] Furthermore, they assign gaps opening throughout the Brillouin zone as arising from scattering from {330}, {411} as well as {420}, {332}, and {422} planes, while it is the distortion of the atomic planes with respect to the body-centered cubic (bcc) structure in real space that enhances the scattering from the {411}, especially, and {330} planes. Subsequently, Mizutani et al. have analyzed the free electron bands and argue that the {330} and {411} planes have the dominant role in creating a declining slope of the density of states curve at the Fermi level.[17,19−23] Unfortunately, existing arguments based on the nearly free electron model and other related approaches of electronic structure for metals do not address the chemical structure of these intermetallics, that is, how the various atoms are arranged.[24−26]

In this paper, we report the crystal structures of five different $Cu_{5-x}Zn_{8+x}$ samples for $x = -0.59(3)$, $-0.31(3)$, 0.00(3), 0.44(3), and 0.79(3) with the cubic γ-brass structure, as refined by both neutron and X-ray powder diffraction. This range corresponds to the existence of the γ-brass structure (57−68 atom % Zn) in the Cu−Zn phase diagram, shown in Figure 1. Our crystallographic work focuses on the "coloring problem"[29] of Cu and Zn atoms among the different crystallographic sites. Given the similar X-ray scattering factors for Cu and Zn, a combination of X-ray and neutron diffraction is necessary to obtain accurate structural chemical information in these Cu−Zn phases. X-ray and neutron diffraction studies of Cu−Al and Cu−Al−Zn γ-brasses have already been successful at distinguishing site occupancy patterns and structural distortions over the observed composition range.[30,31] The factors influencing one atomic arrangement over another in a solid-state structure are defined by energetic contributions originating from the site potentials and pairwise interatomic potentials. These are, respectively, the *site energy* and the *bond energy*, which can be assessed by a population analysis of the calculated electronic structure.[29] Within the tight-binding approximation, the band energy can be decomposed into

(15) Jones, H. *Proc. R. Soc. London, Ser. A* **1934**, *144*, 225.
(16) Mott, N. F.; Jones, H. *The Theory of the Properties of Metals and Alloys*; Clarendon Press: Oxford,1936.
(17) Mizutani, U.; Takeuchi, T.; Sato, H. *Prog. Mater. Sci.* **2004**, *49*, 227.
(18) Paxton, A. T.; Methfessel, M.; Pettifor, D. G. *Proc. R. Soc. London, Ser. A* **1997**, *453*, 1493.
(19) Mizutani, U.; Asahi, R.; Sato, H.; Takeuchi, T. *Philos. Mag.* **2006**, *86*, 645.
(20) Asahi, R.; Sato, H.; Takeuchi, T.; Mizutani, U. *Phys. Rev. B: Condens. Mat. Mater. Phys.* **2005**, *B72*, 125102.
(21) Asahi, R.; Sato, H.; Takeuchi, T.; Mizutani, U. *Phys. Rev. B: Condens. Mat. Mater. Phys.* **2005**, *B71*, 165103.
(22) Mizutani, U.; Takeuchi, T.; Sato, H. *J. Non-Cryst. Solids* **2004**, *334 & 335*, 331.
(23) Takeuchi, T.; Sato, H.; Mizutani, U. *J. Alloys Compd.* **2002**, *342*, 355.
(24) Schubert, K. *Z. Metallkd.* **1989**, *80*, 783.
(25) Johnson, O. *Bull. Chem. Soc. Jpn.* **1973**, *46*, 1929.
(26) Bradley, A. J. *Physica* **1949**, *15*, 170.
(27) Massalski, T. B. In *Binary Alloy Phase Diagrams*, 2nd ed.; Massalski, T. B., Okamoto, H., Subramanian, P. R., Kacprzak, L., Eds.; ASM International: Materials Park, OH, 1990; Vol. 3, p 3068.
(28) Amar, H.; Johnson, K. H.; Wang, K. P. *Phys. Rev.* **1966**, *148*, 672.
(29) Miller, G. J. *Eur. J. Inorg. Chem.* **1998**, 523.
(30) Kisi, E. H. *Mater. Sci. Forum* **1988**, *27−28*, 89.
(31) Kisi, E. H.; Browne, J. D. *Acta Crystallogr., Sect. B* **1991**, *B47*, 835.

the sum of *site energy* and *bond energy* terms according to eq 1

$$E_{\text{Band}} = E_{\text{Site}} + E_{\text{Bond}} = (\sum_i q_i\alpha_i)_{\text{Site}} + (\sum_{i\neq j} p_{ij}\beta_{ij})_{\text{Bond}} \quad (1)$$

where α_i and β_{ij} are coulomb and resonance integrals, q_i values are the orbital occupation numbers, and p_{ij} values are the overlap populations involving orbitals i and j. To analyze these contributions in the Cu−Zn system and to identify the chemical parameters consistent with the specific ordering, tight-binding, linear muffin-tin orbital calculations within the atomic sphere approximation (TB-LMTO-ASA)[32] have been carried out on the series $Cu_{5.59}Zn_{7.41}$, $Cu_{5.31}Zn_{7.69}$, $Cu_{5.00}Zn_{8.00}$, $Cu_{4.56}Zn_{8.44}$, and $Cu_{4.21}Zn_{8.79}$. We also performed similar ab initio calculations on the β-brass CuZn phase in order to interrogate the phase diagram boundaries between the β and γ phases. We believe this combination of structural and theoretical analysis provides some new insights into the behavior of these Hume−Rothery phases.

Experimental Section

A. Synthesis and Chemical Analysis. Five different Cu−Zn samples were targeted by combining the pure elements, copper (powder, Fisher, 99.999%) and zinc (powder, Fisher, 99.999%), in the Zn atomic percentages of 57.0, 59.0, 61.5, 65.0, and 67.5. The alloys were annealed at 1073 K in evacuated silica tubes for 2 days, then slowly cooled to 900 K, and finally quenched in water to prevent any formation of superstructure or long-range ordering at lower temperatures.[33,34] Indeed, in the similar Zn−Pd system we recently observed that long-range ordered modulated structures in these γ-brass systems might be synthesized by slow cooling.[9,10] The Cu−Zn samples are stable upon exposure to air and water. Electron microprobe analyses were performed using a JEOL JXA-8200 and with the pure elements as standards to obtain quantitative values. These analytical results are summarized in Table 1, which shows excellent agreement with both the loaded compositions and those refined from subsequent diffraction experiments.

B. Crystal Structure Determination by Powder Diffraction. B1. X-ray Diffraction: X-ray powder diffraction patterns of these phases were recorded on a Rigaku Ultima III diffractometer mounted on a sealed tube generator with a Cu target, using $K\alpha_1$ and $K\alpha_2$ radiations. Data were collected at 0.02° steps for 5 s/step over the 2θ range 5−90°. Figure 2a shows the observed and calculated patterns along with the difference curve for $Cu_{4.21}Zn_{8.79}$. Figure 2b shows the five diffraction patterns in the 2θ range 42−50°. The slightly shifting diffraction peaks as the composition changes indicate the changing unit cell sizes along the series. On the basis of the structural arrangement known from the literature for the γ-brass Cu−Zn phase,[35−37] the unit cell parameters and the atomic positions of $Cu_{5.59}Zn_{7.41}$, $Cu_{5.31}Zn_{7.69}$, $Cu_{5.00}Zn_{8.00}$, $Cu_{4.56}Zn_{8.44}$, and $Cu_{4.21}Zn_{8.79}$ were successfully refined with the Rietveld method, using the JANA2000 program with 61 parameters.[38] This confirms the symmetry, space group, and cell parameters of these five γ-brass phases. All five intermetallic phases have the bcc space group, $I\bar{4}3m$, with four formula units per cell. Table 1 summarizes the unit cell parameters and refinement results; Table 2 lists the refined atomic positions and equivalent isotropic displacement parameters.

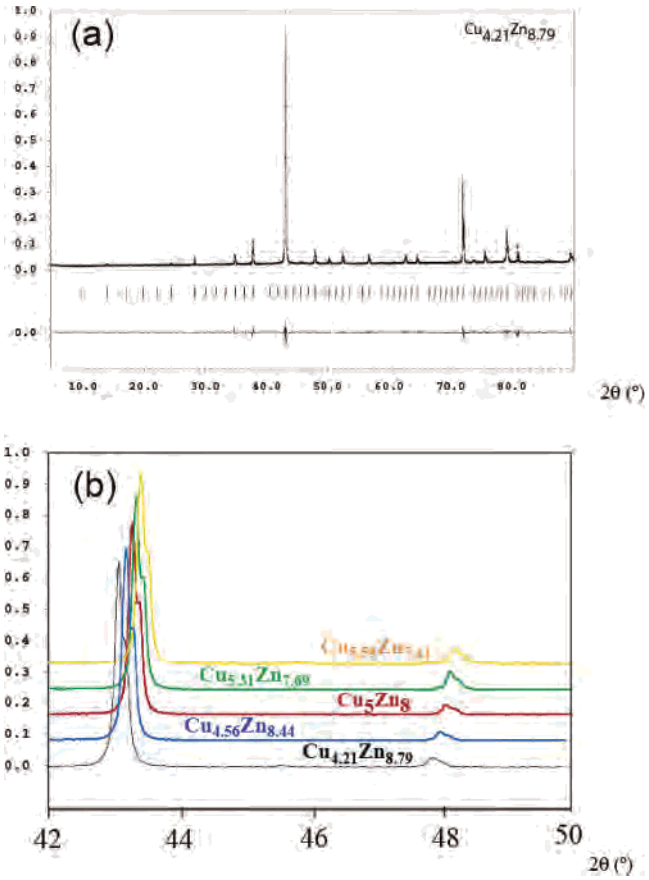

Figure 2. (a) Observed and calculated X-ray powder diffraction patterns of $Cu_{4.21}Zn_{8.79}$ for the 2θ range 5−90°. The intensity scale is normalized to the most intense reflection ({330} and {411}). The difference curve is also illustrated on the same scale. (b) X-ray powder diffraction patterns in the 2θ range 42−50° observed for $Cu_{5.59}Zn_{7.41}$, $Cu_{5.31}Zn_{7.69}$, $Cu_{5.00}Zn_{8.00}$, $Cu_{4.56}Zn_{8.44}$, and $Cu_{4.21}Zn_{8.79}$.

B2. Neutron Diffraction: Since the scattering factors for Cu and Zn may not permit distinguishing these atoms by X-ray powder diffraction (just one electron difference), neutron powder diffraction was carried out on these compounds. Indeed, the elastic neutron cross sections for Cu (7.718×10^{-24} cm^2) and Zn (5.680×10^{-24} cm^2) are significantly different to allow us to refine site distributions. Time-of-flight (TOF) neutron diffraction data were collected at ambient conditions on the Neutron Powder Diffractometer (NPDF) at the Manuel Lujan Neutron Scattering Center of Los Alamos National Laboratory. This instrument is a high-resolution powder diffractometer located at flight path 1, 32 m from the spallation neutron target. The data were collected at 295 K using the 148°, 119°, 90° and 46° banks, which cover a *d*-spacing range from 0.12 to 7.2 Å. Figure 3 illustrates the observed and calculated neutron diffraction patterns for $Cu_{4.21}Zn_{8.79}$ as an example.

The structure was refined using the General Structure Analysis System, a Rietveld profile analysis program developed by Larson and Von Dreele.[39] The starting structural models for each composi-

(32) Andersen, O. K. *Phys. Rev. B* **1986**, *B34*, 2439.
(33) Morton, A. J. *Acta Metall.* **1979**, *27*, 863.
(34) Morton, A. J. *Phys. Status Solidi A* **1974**, *23*, 275.
(35) Brandon, J. K.; Brizard, R. Y.; Chieh, P. C.; McMillan, R. K.; Pearson, W. B. *Acta Crystallogr., Sect. B* **1974**, *30*, 1412.
(36) Von Heidenstam, O.; Johansson, A.; Westman, S. *Acta Chem. Scand.* **1968**, *22*, 653.
(37) Bradley, A. J.; Thewlis, J. *Proc. R. Soc. London* **1926**, *112A*, 678.
(38) Petricek, V.; Dusek, M. *The Crystallographic Computing System JANA2000*; Institute of Physics: Praha, Czech Republic, 2000.
(39) Larson, A. C.; Dreele, R. B. V. GSAS, *Generalized Structure Analysis System*; LANSCE: Los Alamos, NM, 2004.

Table 2. Fractional Atomic Coordinates, Site Occupation Factors (SOF), and Equivalent Isotropic Displacement Parameters for $Cu_{5-x}Zn_{8+x}$ ($x = -0.59$, -0.31, 0.00, 0.44, and 0.79) As Refined by Neutron and X-ray (in *italics*) Powder Diffraction

sites	SOF (Cu/Zn)	*x*	*y*	*z*	U_{eq}
		$Cu_{5.59}Zn_{7.41}$			
M1 (8*c*)	1/0	0.82789(7)	0.82789(7)	0.82789(7)	0.0127(2)
		0.82878(5)	*0.82878(5)*	*0.82878(5)*	*0.0154(4)*
M2 (8*c*)	0/1	0.10797(6)	0.10797(6)	0.10797(6)	0.0128(3)
		0.10791(5)	*0.10791(5)*	*0.10791(5)*	*0.0162(5)*
M3 (12*e*)	1/0	0.35581(8)	0	0	0.0156(4)
		0.3600(4)			*0.0182(5)*
M4 (24*g*)	0.10(2)/0.90(2)	0.31162(4)	0.31162(4)	0.03666(7)	0.0177(3)
		0.31111(5)	*0.31111(5)*	*0.03644(5)*	*0.0199(4)*
		$Cu_{5.31}Zn_{7.69}$			
M1 (8*c*)	1/0	0.82690(5)	0.82690(5)	0.82690(5)	0.0130(3)
		0.82725(6)	*0.82725(6)*	*0.82725(6)*	*0.0147(3)*
M2 (8*c*)	0/1	0.10792(6)	0.10792(6)	0.10792(6)	0.0137(2)
		0.10775(5)	*0.10775(5)*	*0.10775(5)*	*0.0163(6)*
M3 (12*e*)	1/0	0.35592(6)	0	0	0.0155(2)
		0.3579(5)			*0.0178(5)*
M4 (24*g*)	0.06(1)/0.94(1)	0.31190(6)	0.31190(6)	0.03680(7)	0.0167(4)
		0.31073(5)	*0.31073(5)*	*0.03667(5)*	*0.0202(4)*
		$Cu_{5.00}Zn_{8.00}$			
M1 (8*c*)	1/0	0.82774(6)	0.82774(6)	0.82774(6)	0.0125(2)
		0.82804(5)	*0.82804(5)*	*0.82804(5)*	*0.0144(3)*
M2 (8*c*)	0/1	0.10781(7)	0.10781(7)	0.10781(7)	0.0142(2)
		0.10787(4)	*0.10787(4)*	*0.10787(4)*	*0.0166(6)*
M3 (12*e*)	1/0	0.35579(9)	0	0	0.0177(2)
		0.3582(5)			*0.0187(6)*
M4 (24*g*)	0/1	0.31156(7)	0.31156(7)	0.03674(9)	0.0186(1)
		0.31061(4)	*0.31061(4)*	*0.03683(6)*	*0.0201(4)*
		$Cu_{4.56}Zn_{8.44}$			
M1 (8*c*)	1/0	0.82805(6)	0.82805(6)	0.82805(6)	0.0101(2)
		0.82799(5)	*0.82799(5)*	*0.82799(5)*	*0.0161(6)*
M2 (8*c*)	0/1	0.10744(5)	0.10744(5)	0.10744(5)	0.0102(3)
		0.10749(4)	*0.10749(4)*	*0.10749(4)*	*0.0165(4)*
M3 (12*e*)	0.85(2)/0.15(2)	0.3573(2)	0	0	0.0147(2)
		0.3569(2)			*0.0175(5)*
M4 (24*g*)	0/1	0.31088(6)	0.31088(6)	0.03687(6)	0.0153(4)
		0.31059(5)	*0.31059(5)*	*0.03677(5)*	*0.0169(5)*
		$Cu_{4.21}Zn_{8.79}$			
M1 (8*c*)	1/0	0.82827(6)	0.82827(6)	0.82827(6)	0.0087(2)
		0.82814(6)	*0.82814(6)*	*0.82814(6)*	*0.0168(5)*
M2 (8*c*)	0/1	0.10737(6)	0.10737(6)	0.10737(6)	0.0097(2)
		0.10743(5)	*0.10743(5)*	*0.10743(5)*	*0.0142(4)*
M3 (12*e*)	0.73(2)/0.27(2)	0.3569(1)	0	0	0.0181(3)
		0.3570(1)			*0.0178(4)*
M4 (24*g*)	0/1	0.31032(7)	0.31032(7)	0.03651(7)	0.0141(2)
		0.31041(6)	*0.31041(6)*	*0.03654(5)*	*0.0193(6)*

tion came from the X-ray refinements. Each model was refined using the four banks simultaneously (148°, 119°, 90°, and 46° banks) for unit cell parameters, atomic positions, and equivalent isotropic displacement parameters. Background coefficients, scale factors, isotropic strain terms in the profile function, and sample absorption were also refined for a total of 61 parameters. In order to elucidate the arrangement and concentration of Cu and Zn, we allowed the occupancies to be refined. After relaxation of the occupancies, the refinements smoothly converged to solutions where specific mixed Cu/Zn sites are listed in Table 2. The refined chemical compositions are generally within 2 atom % of the loaded composition and microprobe analyses. The unit cell parameters, atomic positions, isotropic thermal displacement parameters, and refined sites occupancies are listed in Table 2.

Structural Discussion

The five $Cu_{5-x}Zn_{8+x}$ specimens, $x = -0.59$, -0.31, 0.00, 0.44, and 0.79, crystallize in the cubic γ-brass structure, and their cubic lattice parameters vary linearly with composition, as shown in Figure 4. These data also reveal a typical volume

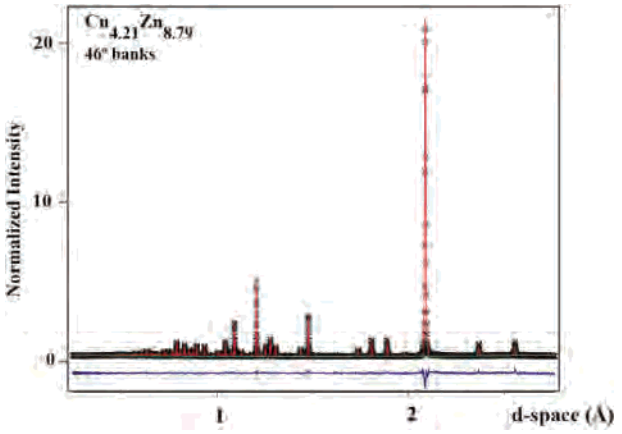

Figure 3. TOF neutron powder diffraction patterns for *d*-spacings between 0.25 and 2.75 Å for $Cu_{4.21}Zn_{8.79}$ taken from data obtained with the 46° bank detectors. Observed data are represented by crosses; calculated results are represented by the red line. The intensity scale uses arbitrary units. The difference curve is illustrated in blue on the same scale.

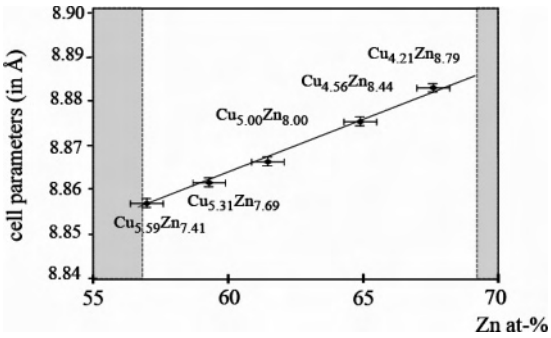

Figure 4. Variation in unit cell parameters for the cubic γ-brass phases $Cu_{5-x}Zn_{8+x}$ ($x = -0.59$, -0.33, 0.00, 0.45, and 0.77) with Zn composition, represented as percent composition Zn, as refined from powder neutron diffraction data. The dashed lines identify the limits of the composition range where the γ-brass phases in the Cu−Zn diagram are observed. Standard deviations for the atomic occupation and the unit cell parameters are represented.

compression for these binary Cu−Zn phases as compared to a linear variation of volume based upon the pure elements Cu and Zn.[10] In addition, there is a linear variation in the valence s, p electron density with composition for these γ-brass phases according to the expression ρ_{sp} ($e^-/Å^3$) = $0.0807 + 0.0668f_{Zn}$, where f_{Zn} = fraction of Zn in the sample. These linear relationships corroborate the refined site occupancies and resulting compositions and argue against vacancies in these structures according to our synthetic procedures.

The cubic γ-brass structure is a relatively complicated one having 52 atoms in the unit cell. Various descriptions have been proposed in the past. The most traditional one involves the 26-atom cluster constructed from successive polyhedral shells: (a) an inner tetrahedron of M2 atoms; (b) an outer tetrahedron of M1 atoms sitting above the faces of the inner tetrahedron; (c) an octahedron of M3 atoms lying above the edges of the outer tetrahedron; (d) a distorted cuboctahedron of M4 atoms placed above the edges of the octahedron (Figure 5). These polyhedra adopt a bcc packing; this classical description begins from a modified $3 \times 3 \times 3$ superstructure of a bcc packing of atoms, i.e., the β-brass structure, as pointed out in the introduction.

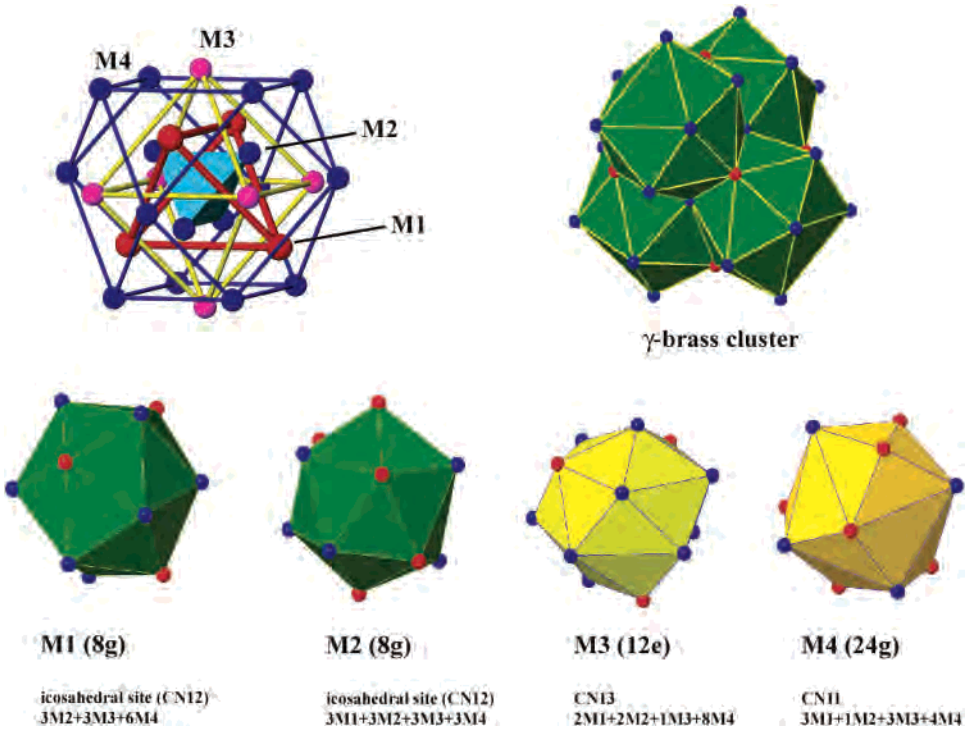

Figure 5. Representations of the cubic γ-brass structure of $Cu_{5-x}Zn_{8+x}$ ($x = -0.59, -0.33, 0.00, 0.45$, and 0.77): blue spheres, Zn atoms; red spheres, Cu atoms. (top left) Representation of the 26-atom cluster that forms a bcc-type packing, emphasizing the different polyhedra. (top right) Four condensed M1-centered icosahedra. (bottom) Local environment for each of the four atomic sites of the γ-brass structure.

Another description of this structure involves the local environments at each of the four distinct crystallographic sites, which are illustrated in Figure 5 using a distance cutoff of 2.9 Å. The M1 and M2 sites are coordinated by distorted icosahedra, whereas the M3 and M4 sites show 13-atom and 11-atom coordination environments, respectively. Four M1 sites forming the outer tetrahedron in the 26-atom cluster and their coordinating icosahedra create another possible fundamental building block for the γ-brass structure: four interpenetrating M1-centered icosahedra,[40] which can be formulated as $[M1(M2_{3/3}M3_{3/2}M4_{6/2})]_4$. A survey of the interatomic distances, listed in Table 3, indicates that the two icosahedral sites, M1 and M2, have shorter average distances to their coordinating atoms than those for the M3 and M4 sites. Likewise, the M1 and M2 have lower isotropic displacement parameters than the M3 and M4 sites (see Table 2). The relative complexity of the atomic structure and the presence of these icosahedra highlight the quasi-crystal approximant character of this phase.

For the ideal composition Cu_5Zn_8, the M1 and M3 sites are fully occupied by Cu atoms, whereas the M2 and M4 sites are fully occupied by Zn atoms; i.e., the 26-atom cluster is formulated as $\{[Zn_4Cu_4](Cu)_6(Zn)_{12}\}$. This distribution pattern leads to shorter (on average) heteronuclear Cu−Zn distances and longer homonuclear Cu−Cu and Zn−Zn distances in Cu_5Zn_8. As the chemical composition varies, our neutron diffraction results indicate that substitutions are restricted to either the M3 or M4 sites, with the specific tendency depending upon how the composition changes—there is no redistribution of Cu and Zn among the M3 and M4 sites. With respect to the 26-atom, "classical" γ-brass cluster, the inner and outer tetrahedra are completely occupied by Zn and Cu atoms, respectively, creating a $[Zn_4Cu_4]$ tetrahedral star core; variations in composition occur

Table 3. Interatomic Distances in $Cu_{5-x}Zn_{8+x}$ ($x = -0.59, -0.31, 0.00, 0.44$, and 0.79) As Determined from Neutron Powder Diffraction at 298 K

	$Cu_{5.59}Zn_{7.41}$	$Cu_{5.31}Zn_{7.69}$	$Cu_{5.00}Zn_{8.00}$	$Cu_{4.56}Zn_{8.44}$	$Cu_{4.21}Zn_{8.79}$
M1−M4 (×3)	2.5440(8)	2.5466(7)	2.5810(9)	2.5445(8)	2.5947(9)
M4 (×3)	2.5873(7)	2.5775(7)	2.6114(8)	2.5930(8)	2.6077(8)
M2 (×3)	2.6074(8)	2.6207(7)	2.6314(9)	2.6083(7)	2.6261(8)
M3 (×3)	2.7007(7)	2.7074(5)	2.7037(9)	2.7135(11)	2.6976(8)
average	2.6098(8)	2.6346(7)	2.6319(9)	2.6329(9)	2.6315(8)
M2−M3 (×3)	2.5781(6)	2.5804(7)	2.5465(9)	2.5952(9)	2.5402(8)
M1 (×3)	2.6074(8)	2.6207(7)	2.5881(8)	2.6083(7)	2.6015(8)
M4 (×3)	2.6277(7)	2.6327(8)	2.6114(8)	2.6289(7)	2.6077(8)
M2 (×3)	2.7046(8)	2.7048(8)	2.7043(7)	2.6968(6)	2.7129(7)
average	2.6294(8)	2.6131(7)	2.6126(8)	2.6148(9)	2.6156(8)
M3−M4 (×2)	2.5444(6)	2.5417(6)	2.5477(8)	2.5328(10)	2.5423(13)
M3 (×1)	2.554(1)	2.5534(8)	2.5572(11)	2.5526(8)	2.5640(7)
M2 (×2)	2.5781(8)	2.5804(7)	2.5810(9)	2.5952(11)	2.5947(9)
M1 (×2)	2.7007(8)	2.7074(6)	2.7043(7)	2.7135(11)	2.7129(8)
M4 (×4)	2.8063(4)	2.8102(6)	2.8091(6)	2.8086(6)	2.8062(7)
M4 (×2)	2.8517(6)	2.8505(6)	2.8561(8)	2.8589(11)	2.8676(8)
average	2.7022(8)	2.7042(6)	2.7055(8)	2.7083(9)	2.7095(9)
M4−M3 (×1)	2.5440(8)	2.5417(7)	2.5465(9)	2.5445(8)	2.5402(8)
M1 (×1)	2.5444(6)	2.5466(7)	2.5477(8)	2.5526(10)	2.5640(9)
M1 (×1)	2.5873(9)	2.5775(8)	2.5881(10)	2.5930(8)	2.6015(8)
M2 (×1)	2.6277(7)	2.6327(8)	2.6314(9)	2.6289(7)	2.6261(8)
M4 (×4)	2.6399(7)	2.6406(8)	2.6433(10)	2.6487(8)	2.6527(9)
M3 (×2)	2.8063(4)	2.8102(6)	2.8091(6)	2.8086(6)	2.8062(7)
M3 (×1)	2.8517(6)	2.8505(6)	2.8561(8)	2.8589(12)	2.8676(8)
average	2.6662(7)	2.6665(7)	2.6692(8)	2.6718(8)	2.6748(8)

(40) Lord, E. A.; Ranganathan, S. *J. Non-Cryst. Solids*, **2004**, *334 & 335*, 121.

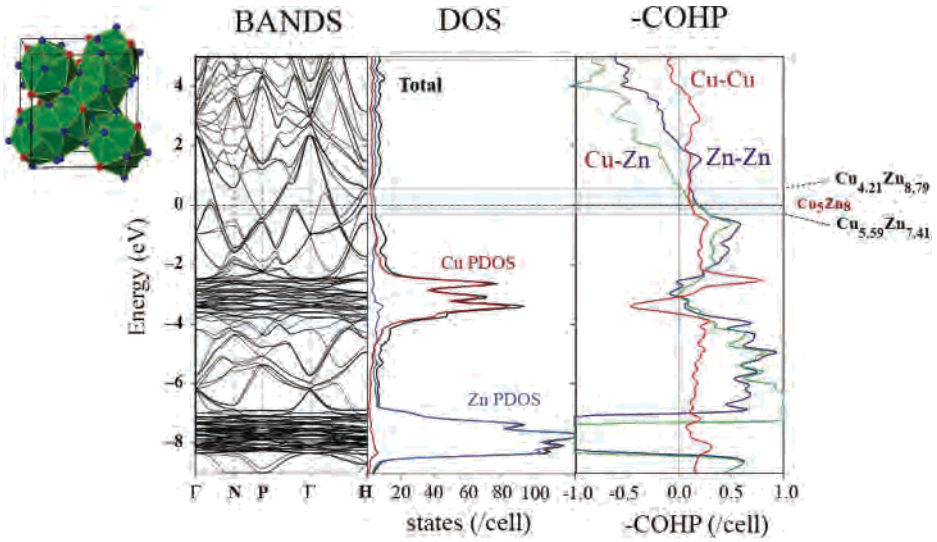

Figure 6. Energy bands, total and partial Cu (red) and Zn (blue) DOS curves, and COHP Cu−Zn (red) and Zn−Zn (blue) curves for Cu_5Zn_8 in the cubic γ-brass structure. The Fermi level (dashed line) is the energy reference. Fermi levels for upper and lower composition limits in $Cu_{5-x}Zn_{8+x}$ ($x = -0.59$ and 0.79) are indicated by the gray region. In the COHP curves, bonding interactions occur for −COHP > 0 and antibonding interactions occur for −COHP < 0.

at the outer regions of this cluster, i.e., the M3 and M4 sites, exclusively. The 26-atom cluster can be formulated as $\{[Zn_4Cu_4](M3)_6(M4)_{12}\}$. Relative to Cu_5Zn_8, Cu-rich species give $\{[Zn_4Cu_4](Cu)_6(Cu_uZn_{1-u})_{12}\}$ and Zn-rich species give $\{[Zn_4Cu_4](Cu_{1-v}Zn_v)_6(Zn)_{12}\}$. Closer examination of the interatomic distances associated with the M1 and M2 sites reveals an interesting relationship between atomic distributions and distances: in the Cu-rich species ($Cu_{5+6u}Zn_{8-6u}$), Cu substitutes at the M4 sites, which have the shortest distances to the M1 (Cu) sites and the longest distances to the M2 (Zn) sites; in the Zn-rich species ($Cu_{5-3v}Zn_{8+3v}$), Zn substitutes at the M3 sites, which have the longest distances to the M1 (Cu) sites and the shortest distances to the M2 (Zn) sites.

Electronic Structure Calculations

To understand the relative stability of the γ-brass phase from a chemical perspective as well as the specific site substitution patterns for Cu and Zn and composition range in $Cu_{5-x}Zn_{8+x}$ phases, electronic structure calculations have been carried out on various γ-brass and β-brass models in the Cu−Zn system with TB-LMTO-ASA[32] using the LMTO, version 4.7, program.[41] In this approach, exchange and correlation were treated in a local density approximation.[42] All relativistic effects except spin−orbit coupling were taken into account using a scalar relativistic approximation.[43] The radii of the Wigner−Seitz (WS) spheres were obtained by requiring the overlapping potential to be the best possible approximation to the full potential according to an automatic procedure; no empty spheres were necessary.[44] The WS radii determined by this procedure were 1.42 Å for Cu and 1.53 Å for Zn. The basis sets included 4s, 4p, and 3d orbitals for Cu and Zn. The **k**-space integrations to determine self-consistent charge densities, densities of states (DOS), and crystal orbital Hamilton populations (COHP)[45] were performed by an improved tetrahedron method[46] on grids of 400−600 **k**-points of the corresponding irreducible wedges of the first Brillouin zones.

γ-$Cu_{5-x}Zn_{8+x}$: Figure 6 illustrates the energy bands and the DOS and COHP curves for Cu−Zn, Cu−Cu, and Zn−Zn interatomic contacts of Cu_5Zn_8 in a 14 eV energy window surrounding the Fermi level. The partial DOS curves of the Cu and Zn contributions are represented in red and blue, respectively. The 4s and 4p orbitals of Cu and Zn form broad, nearly free electron-like energy bands. A large peak around 7.5 eV below the Fermi level mainly arises from Zn 3d states overlapping with Cu 4p wavefunctions, whereas between 2.5 and 4 eV below the Fermi level, a broader peak is identified to be mostly Cu 3d states overlapping with Zn valence 4p orbitals. Between 0.5 eV below and above the Fermi level, the DOS curve shows a significant reduction in value, i.e., a pseudogap that is primarily caused by d−p hybridization. Assuming a rigid-band approximation, we have located the Fermi levels for $Cu_{5.59}Zn_{7.41}$ (150.4 e^-; vec = 1.570, 57.0 atom % Zn) and $Cu_{4.21}Zn_{8.79}$ (151.8 e^-; vec = 1.676; 67.6 atom % Zn) on this DOS curve by the gray window. These boundaries correspond very well with the limits of the pseudogap and also identify the upper and lower limits for the existence of the γ-brass structure in the Cu−Zn diagram (see Figures 1 and 4).

(41) Krier, G.; Jepsen, O.; Burkhardt, A.; Andersen, O. K. *Tight-Binding LMTO, version 4.7*; Max-Planck-Institut für Festkörperforschung: Stuttgart, Germany, 1997.
(42) von Barth, U.; Hedin, L. *J. Phys. C: Solid State Phys.* **1972**, *5*, 1629.
(43) Koelling, D.; Harmon, B. N. *J. Phys. C: Solid State Phys.* **1977**, *10*, 3107.
(44) Jepsen, O.; Andersen, O. K. *Z. Phys. B: Condens. Matter* **1995**, *97*, 645.
(45) Dronskowski, R.; Blöchl, P. E. *J. Phys. Chem.* **1993**, *97*, 8617.
(46) Blöchl, P. E.; Jepsen, O.; Andersen, O. K. *Phys. Rev. B: Condens. Matter* **1994**, *B49*, 16223.

Table 4. Various Atomic Arrangements for Cu_5Zn_8 within the Cubic γ-Brass Structure and Their Relative Total Energies per Atom (eV)[a]

	space group	M1 (M1′)	M2 (M2′)	M3 (M3′)	M4 (M4′)	formula	energy/atom (eV)
A	$I\bar{4}3m$	Cu	Zn	Cu	Zn	$(Cu_{10}Zn_{16})_2$	0
B	$I\bar{4}3m$	Zn	Cu	Cu	Zn	$(Cu_{10}Zn_{16})_2$	0.028
C	$P\bar{4}3m$	Cu	Zn	Cu	Zn	$(Cu_{10}Zn_{16})$	0.010
		Zn	Cu	Cu	Zn	$(Cu_{10}Zn_{16})$	
D	$P\bar{4}3m$	Cu	Cu	Zn	Zn	(Cu_8Zn_{18})	0.025
		Zn	Zn	Zn	Cu	$(Cu_{12}Zn_{14})$	
E	$P\bar{4}3m$	Cu	Cu	Cu	Zn	(Cu_6Zn_{20})	0.025
		Zn	Zn	Cu	Zn	$(Cu_{14}Zn_{12})$	
F	$P\bar{4}3m$	Cu	Zn	Zn	Zn	(Cu_4Zn_{22})	0.001
		Cu	Zn	Zn	Cu	$(Cu_{16}Zn_{10})$	
G	$P\bar{4}3m$	Zn	Cu	Zn	Zn	(Cu_4Zn_{22})	0.012
		Zn	Cu	Zn	Cu	$(Cu_{16}Zn_{10})$	
H	$P\bar{4}3m$	Zn	Zn	Zn	Zn	(Cu_0Zn_{26})	0.022
		Cu	Cu	Zn	Cu	$(Cu_{20}Zn_6)$	

[a] Models adopting the $P\bar{4}3m$ space group have two inequivalent sets of sites.

In the energy band structure, significant band gaps across the Fermi level for Cu_5Zn_8 are mostly seen at the high symmetry points N ($^1/_2$, $^1/_2$, 0) and Γ (0, 0, 0). In the Pd−Zn system, we have observed the existence of lattice modulations along the [110] directions, which suggests that the fraction of occupied states along the ΓN direction in the Brillouin zone significantly influences the observed γ-brass structures.[10] Furthermore, the upper bound of the pseudogap corresponds to the bottom of parabolic ("free-electron-like") bands at points N and H ($^1/_2$, $-^1/_2$, $^1/_2$). The Cu−Zn COHP curve identifies the upper bound point as the energy (Fermi level) that optimizes heteroatomic pairwise interactions; this energy corresponds to 151.8 valence s, p, and d e^- per formula unit, i.e., $Cu_{4.21}Zn_{8.79}$. While the heteroatomic interactions are optimized at this electron count, both the Cu−Cu and Zn−Zn interactions remain weakly bonded. Therefore, increasing substitution of Cu by Zn in $Cu_{5-x}Zn_{8+x}$ will eventually populate Cu−Zn antibonding states first in the γ-brass structure and lead to structural instability. Regarding the lower limit (Cu-rich side), the argument is less clear, although we observe that the Cu−Zn and Zn−Zn interactions are strongly bonding at ca. 0.7 eV below the Fermi level. Depopulating these bonding states by continuing to increase the Cu concentration will also lead to structural instability. Thus, the range of the pseudogap in the DOS for $Cu_{5-x}Zn_{8+x}$ can be attributed to significant changes in pairwise orbital interactions.

Before considering various substitution patterns on the γ-brass structure, we address the distribution of Cu and Zn atoms in stoichiometric Cu_5Zn_8. TB-LMTO-ASA calculations on various distributions within the cubic cell, listed in Table 4, give the lowest energy arrangement (**A**) in exact agreement with structural characterizations: Cu in M1 and M3 sites, Zn in M2 and M4 sites, space group $I\bar{4}3m$. The highest energy configuration is also bcc but with Cu and Zn atoms switching the inner and outer tetrahedron sites, M1 and M2 (**B**). Another low-energy configuration (**F**) is a primitive cubic arrangement that maintains $[Zn_4Cu_4]$ tetrahedral stars at the corners and center of the unit cell but modifies the distribution of Cu and Zn atoms at the M3 and M4 sites. The integrated COHP values for all pairwise interactions less than 2.90 Å indicate that the high energy arrangement **B** creates significant repulsive (antibonding) Zn−Zn interactions between the M1 and M4 sites, the distances of which are two of the shortest in the entire structure. In the observed arrangement **A**, these M1−M4 contacts are Cu−Zn and attractive (net bonding). Thus, there is an important *bond energy* contribution to the "coloring" of the γ-brass structure.

On the other hand, the TB-LMTO-ASA method is not well-suited to address the *site energy* contribution due to the tails of the wavefunctions that contribute to integrated "charges" within each WS sphere. We can analyze the significance of this term, however, by utilizing semiempirical, extended Hückel theory (EHT) to calculate relative atomic Mulliken populations.[47−50] Relative atomic Mulliken populations for each crystallographic site in a structure ($\langle Q\rangle - Q_{site}$) are evaluated by setting the atomic orbital parameters to be the same for every site in the crystal structure and calculating the difference between the calculated site population at each site (Q_{site}) and the average value overall sites ($\langle Q\rangle$) for a range of valence electron counts. In this way, when the relative atomic Mulliken population at a site is negative, then the site is attractive for greater than average valence electron density; when it is positive, then the site is attractive for lower than average valence electron density. For this calculation on the Cu−Zn γ-brass structure, we do not include the valence 3d atomic orbitals on Cu or Zn because both are formally filled as seen in the DOS curve in Figure 6 but, rather, utilize just the 4s and 4p atomic orbitals, which are expressed as single-ζ Slater-type orbitals in EHT. Including the valence 3d orbitals changes the quantitative but not the qualitative results of the calculations. Diagonal Hamiltonian matrix elements are given by valence state orbital energies derived from atomic spectra for Zn; off-diagonal Hamiltonian matrix elements are approximated by the weighted Wolfsberg−Helmholz approximation.[50] The atomic parameters are as follows: Zn 4s, $H_{ii} = -12.41$ eV, $\zeta_1 = 2.01$; Zn 4p, $H_{ii} = -6.53$ eV, $\zeta_1 = 1.70$. With the use of the monatomic model, the relative Mulliken populations[51−54] for the four crystallographic sites are plotted in Figure 7 as a function of vec; such plots were valuable for predicting site preferences for Mg, Zn, and Al in quasi-crystal approximant Bergman phases.[51,52] For the range of observed γ-brass structures, the M2 and M4 sites clearly attract the greater valence electron density, while the M1 and M3 sites attract the lower valence electron density. Within the approximation of filled 3d orbitals at both Cu and Zn for these intermetallics, Zn has greater valence electron density than Cu, such that

(47) Hoffmann, R. *Solids and Surfaces: A Chemist's View of Bonding in Extended Structures*; VCH: New York, 1988.
(48) Hoffmann, R. *J. Chem. Phys.* **1963**, *39*, 1397.
(49) Burdett, J. K. *Chemical Bonding in Solids*; Oxford University Press: New York, 1995.
(50) Ammeter, J. H.; Bürgi, H. B.; Thibeault, J. C.; Hoffmann, R. *J. Am. Chem. Soc.* **1978**, *100*, 3686.
(51) Lee, C. S.; Miller, G. J. *J. Am. Chem. Soc.* **2000**, *122*, 4937.
(52) Lee, C. S.; Miller, G. J. *Inorg. Chem.* **2001**, *40*, 338.
(53) Nordell, K. J.; Miller, G. J. *Angew. Chem.* **1997**, *109*, 2098.
(54) Häussermann, U.; Amerioun, S.; Eriksson, L.; Lee, C. S.; Miller, G. J. *J. Am. Chem. Soc.* **2002**, *124*, 4371.

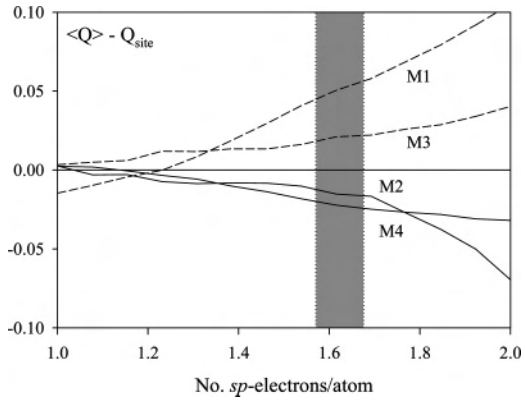

Figure 7. Relative Mulliken populations ($\langle Q \rangle - Q_{site}$) for the four crystallographic sites in the γ-brass structure as a function of vec. Positive values indicate sites for more electropositive elements; negative values indicate sites for more electronegative elements. The gray region marks the range of observed vec values for $Cu_{5-x}Zn_{8+x}$.

Scheme 1

$I\bar{4}3m$		$P222$	$I\bar{4}3m$		$P222$
M1 (8*g*)	⟶	M1a (4*u*)	M2 (8*g*)	⟶	M2a (4*u*)
		M1b (4*u*)			M2b (4*u*)
		M3a (2*q*)			M4a (4*u*)
		M3b (2*t*)			M4b (4*u*)
M3 (12*e*)	⟶	M3c (2*i*)	M4	⟶	M4c (4*u*)
		M3d (2*l*)	(24*g*)		M4d (4*u*)
		M3e (2*m*)			M4e (4*u*)
		M3f (2*p*)			M4f (4*u*)

Zn would be preferentially attracted to the M2 and M4 sites and Cu to the M1 and M3 sites. In earlier applications of the relative Mulliken populations, the electronegativities of the atomic constituents were used as a guide but do not work for the Cu−Zn system: Cu is more electronegative than Zn,[55] which can be attributed to the filled 3d levels of Zn not found in Cu. However, the 4s orbital energy of Zn is lower than that of Cu. Thus, there are both *site energy* and *bond energy* factors contributing to the observed distribution of Cu and Zn in the observed γ-brass phases.

γ-$Cu_{4.21}Zn_{8.79}$ (Zn-Rich Cases): From the atomic arrangement in stoichiometric Cu_5Zn_8, Zn can replace Cu at either the M1 or M3 sites. To understand the site preference for the additional Zn, the total energies of six different models of a hypothetical "$Cu_{16}Zn_{36}$" ("Cu_4Zn_9" as an approximation to $Cu_{4.21}Zn_{8.79}$) compound were calculated. To conduct this study, all calculations were performed in the space group *P*222, a subgroup of $I\bar{4}3m$, and the WS radii for Cu and Zn were kept constant. Scheme 1 shows the correlation between the various Wyckoff sites of the space groups $I\bar{4}3m$ and *P*222. Table 5 lists the different models of "$Cu_{16}Zn_{36}$" by identifying the sites occupied by the additional Zn atoms (Zn fully occupies all M2 and M4 sites). Notice that our study is not exhaustive of all the possible cases but is just representative. According to the relative total energies, the additional Zn atoms definitely prefer to occupy the M3 (12*e*) sites in the cubic structure, which agrees with our neutron diffraction experiments.

Table 5. Site Occupation Patterns and Relative Total Energies for Substitutions on Cu_5Zn_8

$Cu_{16}Zn_{36}$ (modeling $Cu_{4.21}Zn_{8.79}$)							
models	Zn1	Zn2	Zn3	Zn4	Zn5	Zn6	
sites	M1b	M3a + M3b	M3a +M3c	M3a +M3d	M3a +M3e	M3a +M3f	
ΔeV/atom	0	−0.026	−0.027	−0.045	−0.027	−0.026	
$Cu_{24}Zn_{28}$ (modeling $Cu_{5.59}Zn_{7.41}$)							
models	Cu1	Cu2	Cu3	Cu4	Cu5	Cu6	Cu7
sites	M2a	M4a	M4b	M4c	M4d	M4e	M4f
ΔeV/atom	0	−0.141	−0.141	−0.141	−0.216	−0.141	−0.216

The shapes of the calculated DOS curves for the various models (not presented here) are quite similar to the one in Figure 6, so the factors distinguishing the different models are quite subtle. The major justification of the observed site preference is to strengthen the Cu−Zn and Zn−Zn interactions by occupying additional bonding states. Cu−Cu interactions also become more attractive, but the best model, Zn4, minimizes the number of nearest neighbor Cu−Cu contacts while maximizing the number of Cu−Zn interactions. The Zn−Zn contacts become less repulsive; the filled Zn 3d band creates a net antibonding Zn−Zn interaction, as indicated by its integrated COHP value. Previous studies on factors influencing metal atom distributions in polar intermetallic compounds indicate that heterometallic interactions are favored over homometallic ones, especially when electronegative metals like Ni, Zn, or Au are involved,[53,54,56−58] because these elements tend to develop filled valence d and s bands. The site energy also influences the substitution pattern; the relative Mulliken populations for the M1 and M3 sites suggest that the M3 site is the better alternative for Zn, as this site attracts a lower electron density.

γ-$Cu_{5.59}Zn_{7.41}$ (Cu-Rich Cases): In a similar fashion, we have calculated the total energy of seven models of hypothetical "$Cu_{24}Zn_{28}$" to explore the site preferences for replacing Zn atoms with Cu. These results are also listed in Table 5, and the preferred M4 sites show a larger relative stability than we observed for the Zn-rich cases. The observed substitution pattern also serves to maximize the number of heteroatomic Cu−Zn contacts and lowers the number of Zn−Zn contacts. Although the COHP value for the Zn−Zn interactions is bonding near the Fermi level, it is net antibonding due to the filled 3d orbitals. Furthermore, the pattern maximizes the number of Cu−Cu contacts. The COHP curves for Cu−Cu and Zn−Zn contacts indicates that lowering the Fermi level by Cu substitution will make the Cu−Cu and Zn−Zn interactions less bonded (more repulsive in the case of Zn−Zn; less attractive for Cu−Cu).

(55) Mann, J. B.; Meek, T. L.; Knight, E. T.; Capitani, J. F.; Allen, L. C. *J. Am. Chem. Soc.* **2000**, *122*, 5132.
(56) Gout, D.; Benbow, E.; Gourdon, O.; Miller, G. J. *Inorg. Chem.* **2004**, *43*, 4604.
(57) Han, M.-K.; Morosan, E.; Canfield, P. C.; Miller, G. J. *Z. Kristallogr.—New Cryst. Struct.* **2005**, *220*, 95.
(58) Gout, D.; Barker, T. J.; Gourdon, O.; Miller, G. J. *Chem. Mater.* **2005**, *17*, 3661.

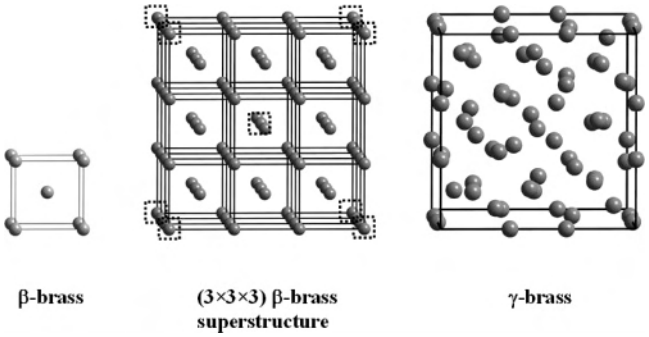

Figure 8. Relationships between the β-brass (left), γ-brass (right), and a $3 \times 3 \times 3$ β-brass-type superstructure (middle) that is related to the γ-brass structure.

γ-Brass vs β-Brass: The γ-brass phase is closely related to the β-brass phase, which corresponds to a bcc structural arrangement with randomly distributed Cu and Zn atoms. Indeed, we can generate the γ-brass arrangement of atoms by starting from a $3 \times 3 \times 3$ superstructure of this β-brass bcc packing of atoms followed by removing 2 atoms from the resulting 54-atom supercell (one from the corner, one from the center of the supercell) and then shifting the remaining atomic sites to the resulting coordinates (see Figure 8). However, this construction involves only the positions of atoms and does not address the distribution of elements: the β-brass phase is completely disordered whereas the γ-brass phase typically shows ordering among the different crystallographic sites.[9,10,35−37] In addition, Paxton et al. have shown that from an electronic structure perspective[18] there is no basis for this description It is, perhaps, important to note here that the cubic γ-brass structure remains unknown for any monatomic system (pure element), although there is a recent report of a Li_{26} cluster found in a Li−Na−Ba phase $Li_{13}Na_{29}Ba_{19}$ that corresponds to the cluster building up the γ-brass structure.[59]

The nearly free electron model accounts quite well for the observed compositions and vec ranges of the bcc-type β-brass structure and the complex cubic γ-brass structure in Hume−Rothery alloys.[17,18] The tight-binding model, which offers some chemical interpretations, is also successful in sorting these two structures within second-moment scaling procedures.[60−62] The general conclusion of these studies is the importance of the DOS with the γ-brass structure showing a distinct lowering of its DOS at the Fermi level for a vec value near 1.7 valence s, p electrons per atom. To further explore this conclusion, we calculated the total DOS curves for four distinct models of γ-brass: (a) the observed structure for Cu_5Zn_8; (b) Cu_5Zn_8 in the defect $3 \times 3 \times 3$ supercell of bcc packing (see Figure 8); (c) a monatomic M_{13} in the γ-brass structure (M═Zn); and (d) M_{13} in the defect $3 \times 3 \times 3$ supercell of bcc packing (see Figure 8). These DOS curves are illustrated in Figure 9 with Fermi levels indicated for vec = 1.57, 1.61, and 1.68, values which correspond to

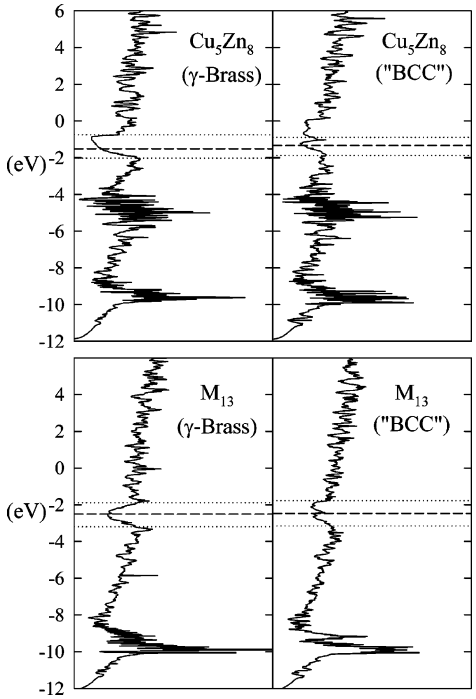

Figure 9. Total DOS curves for four models based upon the γ-brass and β-brass structures. Dashed line indicates Fermi level for vec = 1.61 electrons per atom; dotted lines indicate Fermi levels for upper and lower bounds of vec observed in the Cu−Zn system.

the range of vec observed in the Cu−Zn phase diagram. Clearly, the γ-brass structure creates a deeper pseudogap in the DOS curves near these vec values than the $3 \times 3 \times 3$ supercell of bcc packing does. The chemistry, however, also contributes to deepening that pseudogap even further when the corresponding Cu_5Zn_8 and M_{13} curves are compared. Therefore, we conclude that the pseudogap is associated with the structure itself and the atomic arrangement enhances the gap and through interatomic interactions provides a justification for the atomic distribution.

To further explore the relationship between the bcc-type β-brass with the γ-brass structures, the relative total energies of various $Cu_{1-x}Zn_x$ models were evaluated via a tight-binding approach (TB-LMTO-ASA) and compared. Four different cases were probed: (1) β-brass (bcc-type); (2) γ-brass (52-atom cubic unit cell over 4 crystallographically distinct sites); (3) $2 \times 2 \times 2$ superstructure of the bcc arrangement with vacancies at the corners and center of the cell (14 atoms); and (4) $3 \times 3 \times 3$ superstructure of the bcc arrangement, also with vacancies at the corners and center of the cell (52 atoms). Models 1, 2, and 4 are depicted in Figure 8; model 3 represents an intermediate periodicity between the two observed structural motifs. To account for changes in vec and atomic volumes, the average atomic volumes were modified to reflect the experimental results, whereas the WS radii for Cu and Zn remained constant. Figure 10 illustrates the relative total energies of these models for compositions between 100% Cu to 100% Zn relative to the total energies of the compositionally weighted average from the hypothetical monatomic γ-brasses, "Cu_{13}" and "Zn_{13}". This choice of reference specifically probes the bcc-related structures and the coloring of Cu and Zn through-

(59) Smetana, V.; Babizhetskyy, V.; Vajenine, G. V.; Simon, A. *Angew. Chem., Int. Ed.* **2006**, *45*, 6051.
(60) Burdett, J. K. *Chemical Bonding in Solids*; Oxford University Press: Oxford, 1995.
(61) Hoistad, L.; Lee, S. *J. Am. Chem. Soc.* **1991**, *113*, 8216.
(62) Lee, S. *Acc. Chem. Res.* **1991**, *24*, 249.

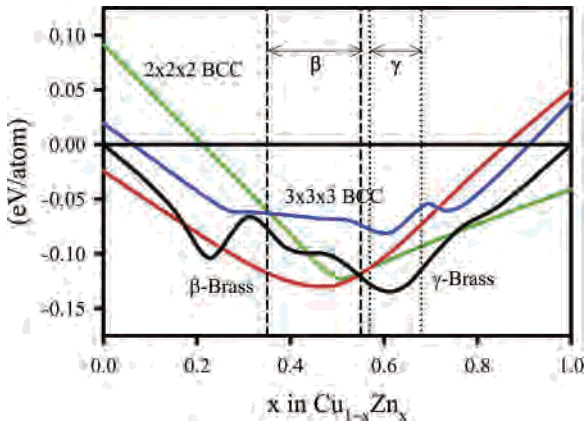

Figure 10. Relative total energies for four models of $Cu_{1-x}Zn_x$: (black line) γ-brass structure; (red line) β-brass structure; (blue line) $3 \times 3 \times 3$ superstructure of the bcc arrangement; and (green line) $2 \times 2 \times 2$ superstructure of the bcc arrangement. The reference is the compositionally weighted average of total energies for hypothetical γ-brasses, "Cu_{13}" and "Zn_{13}." Vertical dotted lines indicate observed compositional width for the Cu−Zn γ-brass structure and dashed lines the Cu−Zn β-brass structure.

out the structures. We have not included the face-centered cubic and hexagonal close-packed (hcp) type structures for comparison.

The agreement with experiment is exceptionally good. These results reiterate the importance of the distortion from a defect-bcc packing of atoms toward stabilizing the γ-brass structure, and the enhancement occurs near 61.5 atom % Zn (vec = 1.615 valence electrons per atom). The $2 \times 2 \times 2$ superstructure was selected for study because there does not seem to be any reason to exclude its existence from the (nearly) free electron model. In fact, using the free electron model to calculate the vec values associated with the first Brillouin zone and the Fermi sphere for this superstructure, we find a lower limit of 1.693 electrons per atom (Fermi sphere) and an upper limit of 2.286 electrons per atom, which lies higher than either the β-brass (1.481−2.000 electrons per atom) or the γ-brass (1.538−1.732 electrons per atom) structures. According to Figure 10, the $2 \times 2 \times 2$ superstructure is energetically competitive near the transition between β- and γ-brasses and then is the preferred structure among these for vec values above ca. 1.75 (this is the range where hcp structures predominate). For all compositions, the $3 \times 3 \times 3$ superstructure never becomes a competitive arrangement. Thus, this tight-binding approach provides an excellent separation of the two brass-type structures and also distinguishes them from reasonable bcc-related models.

Summary

Structural characterization of a series of $Cu_{5-x}Zn_{8+x}$ compounds ($x = -0.59$, -0.31, 0.00, 0.44, and 0.79) with the γ-brass structure shows a specific site distribution pattern around the ideal composition of Cu_5Zn_8. Of the four crystallographic sites, the two that are surrounded by an icosahedral environment and that form $[Zn_4Cu_4]$ tetrahedral stars around the corners and centers of the unit cell refuse chemical substitution for the observed compositional range. This particular substitution pattern has been investigated by electronic structure calculations. These calculations identify influences from both *site energies* and *bond energies* on the observed coloring of this structure over the entire composition range.

Acknowledgment. Part of this work was carried out at the Ames Laboratory, which is operated for the U.S. Department of Energy by Iowa State University under Contract No. W-7405-ENG-82, and was supported by the Materials Sciences Division of the Office of Basic Energy Sciences of the U.S. Department of Energy. This work has also benefited from the use of NPDF at the Lujan Center at Los Alamos Neutron Science Center, funded by the DOE Office of Basic Energy Sciences. Los Alamos National Laboratory is operated by Los Alamos National Security LLC under DOE Contract DE-AC52-06NA25396. The upgrade of NPDF was funded by the NSF through Grant DMR 00-76488. The authors are grateful to Alfred Kracher of the Ames Laboratory for performing electron microprobe analyses on the samples. The authors also wish to thank the reviewers for their thorough review and useful suggestions.

Supporting Information Available: Neutron crystallographic files in CIF format for the structure determination of $Cu_{5.59}Zn_{7.41}$, $Cu_{5.31}Zn_{7.69}$, $Cu_{5.00}Zn_{8.00}$, $Cu_{4.56}Zn_{8.44}$, and $Cu_{4.21}Zn_{8.79}$. This material is available free of charge via the Internet at http://pubs.acs.org.

IC0616380